RUN-TIME ASSESSMENT OF VEHICLE-TERRAIN INTERACTIONS

Robert E. Karlsen* and James L. Overholt
U.S. Army TARDEC,
Warren, MI 48397-5000

Gary Witus
Turing Associates, Inc.
Ann Arbor, MI 48103

ABSTRACT

Military and security operations often require that participants move as quickly as possible, while avoiding harm. Humans judge how fast they can drive, how sharply they can turn and how hard they can brake, based on a subjective assessment of vehicle handling, which results from responsiveness to driving commands, ride quality, and prior experience in similar conditions. Vehicle handling is a product of the vehicle dynamics and the vehicle-terrain interaction. Near real-time methods are needed for unmanned ground vehicles to assess their handling limits on the current terrain in order to plan and execute extreme maneuvers. This paper describes preliminary research to develop on-the-fly procedures to capture vehicle-terrain interaction data and simple models of vehicle response to driving commands, given the vehicle-terrain interaction data.

1. INTRODUCTION

To be effective participants in military and security operations, unmanned ground vehicles (UGV's) will need to operate at the limits of their capabilities. They will need to move and turn as fast as possible, subject to requirements for detecting and avoiding obstacles, for averting overturning, and for reaching waypoints or the destination within some tolerance. UGV motion planning and control has primarily focused on cautious and accurate driving, typically at low speed. The effects of vehicle-terrain interactions on motion and handling have not been adequately addressed.

Movement over uneven terrain produces roll, pitch and yaw accelerations that are collectively referred to as disturbance and are a measure of the "feel of the road". Disturbance is transmitted to on-board driving and obstacle detection sensors. If the sensors have stabilization systems, disturbance can be attenuated but not eliminated. Disturbance reduces the effective range and resolution of sensors by introducing blur and positional uncertainty. UGV's need to limit the disturbance transmitted to these on-board sensors in order to detect obstacles in time to avoid them and to navigate with a desired accuracy. Disturbance also has a significant effect on cornering. Pitch and heave disturbances produce variations in the normal load on the tires or tracks. This can contribute to sideslip during cornering, since periods of low normal load reduce the frictional force needed to make the turn.

For a given vehicle and terrain, the magnitude of the disturbance and its effects depend on the speed and steering angle. Soft soil (e.g., humus and mud), granular surfaces (e.g., sand and gravel), and surfaces with compliant upper layers (e.g. grass or vegetation) all offer resistance to motion. Ground resistance influences fuel consumption and limits the maximum speed a vehicle can achieve. Maximum speed is reached when the ground resistance becomes equal to the tractive force. As previously noted, variations in resistance also produce pitch and yaw disturbances.

The amount of tractive force a vehicle can generate for acceleration or braking is limited by the torque that the vehicle can produce and the frictional force between the running gear and the ground. The friction between the running gear and the terrain also limits lateral acceleration when changing direction. The magnitude of the frictional force depends on the normal load, which can vary on uneven ground. In many terrain types, the coefficient of friction varies with position as the composition of the surface changes, which can have a significant effect on vehicle control. "Spinning out" upon hitting a patch of ice is an extreme example.

A UGV that is able to assess the vehicle-terrain interaction and to predict how it will handle will be able to exercise intelligent mobility planning and control. It will be able to limit its speed to ensure that the sensors can detect obstacles, to self-locate and stop within a given distance, and to ensure that it can turn with a given turning radius. If a prior "map" of the terrain type is available, the UGV will be better able to plan its motion profile to manage power consumption and to plan speed and cornering profiles to more closely track a given path.

Report Documentation Page

Form Approved
OMB No. 0704-0188

1. REPORT DATE	2. REPORT TYPE	3. DATES COVERED
00 DEC 2004	**N/A**	**-**

4. TITLE AND SUBTITLE	5a. CONTRACT NUMBER
Run-Time Assessment Of Vehicle-Terrain Interactions	5b. GRANT NUMBER
	5c. PROGRAM ELEMENT NUMBER
6. AUTHOR(S)	5d. PROJECT NUMBER
	5e. TASK NUMBER
	5f. WORK UNIT NUMBER
7. PERFORMING ORGANIZATION NAME(S) AND ADDRESS(ES) **U.S. Army TARDEC, Warren, MI 48397-5000; Turing Associates, Inc. Ann Arbor, MI 48103**	8. PERFORMING ORGANIZATION REPORT NUMBER
9. SPONSORING/MONITORING AGENCY NAME(S) AND ADDRESS(ES)	10. SPONSOR/MONITOR'S ACRONYM(S)
	11. SPONSOR/MONITOR'S REPORT NUMBER(S)

12. DISTRIBUTION/AVAILABILITY STATEMENT
Approved for public release, distribution unlimited

13. SUPPLEMENTARY NOTES
See also ADM001736, Proceedings for the Army Science Conference (24th) Held on 29 November - 2 December 2005 in Orlando, Florida. , The original document contains color images.

14. ABSTRACT

15. SUBJECT TERMS

16. SECURITY CLASSIFICATION OF:			17. LIMITATION OF ABSTRACT	18. NUMBER OF PAGES	19a. NAME OF RESPONSIBLE PERSON
a. REPORT	b. ABSTRACT	c. THIS PAGE			
unclassified	**unclassified**	**unclassified**	**UU**	**8**	

2. METHODOLOGY

Handling performance is a product of the vehicle-terrain interaction. It is not a terrain property, nor is it a vehicle property. It is a bulk property that can not be measured at an instant in space or time, but can only be measured in aggregate over an interval of space and time.

First-principles multi-body dynamics models are capable of accurately modeling disturbance produced when a vehicle with a compliant suspension travels over uneven terrain. However these models are too complex to run in real time for UGV motion control. They require high-resolution surface elevation data that is generally not available. These models are suitable for relatively uniform and firm surfaces such as roads, but may not adequately describe natural terrain, especially layered terrain and terrain covered by loose particles or vegetation, subject to both elastic and plastic deformation. Prior data on the terrain composition and configuration of the terrain elements is generally not available.

Modeling and simulation efforts in vehicle-terrain interactions, such as ModSAF, CCTT, WARSIM and NRMM, use look-up tables to determine how a vehicle will perform on a given terrain (Birkel, 2003). This typically involves defining multiple categories of terrain and then measuring specific parameters about each of them. To use such an approach in a run-time environment would require sensing characteristics of the terrain and then matching those characteristics to a particular terrain category to obtain the predicted vehicle performance.

Rather than attempt to develop a detailed analytical model of the vehicle-terrain interaction, we follow Brooks' dictum that "the world is its own best model" (Brooks, 1991). Instead of attempting to model the vehicle dynamics and vehicle-terrain interaction, our method is to use the UGV itself as an on-the-fly test instrument. Our approach is to measure handling in the ordinary maneuvers that the vehicle is already performing (thus ensuring that the domain in which we are collecting data is relevant and appropriate) and to add structured perturbations to sense how the vehicle responds. Just as a human driver would tap the brakes, wiggle the steering and momentarily release the throttle to assess response, we propose to add similar perturbations. This approach could also provide a method for obtaining the parameters needed by the more detailed models, such as ModSAF and NRMM. Using a UGV to automatically measure these parameters could reduce much of the tedium in this process.

There are two requirements for the driving command perturbations: (1) they must not significantly affect the vehicle speed or trajectory and (2) they must be sufficient to specify the vehicle-terrain interaction parameters. The study methodology was organized into eight steps:

1. Instrument a test vehicle for the data collection;
2. Design a set of test maneuvers to provide a baseline characterization of the vehicle handling on the terrain;
3. Define a provisional set of driving perturbations to add to the normal driving commands for on-the-fly testing;
4. Collect field data on several types of terrain for the baseline characterization and driving perturbation maneuvers;
5. Analyze the baseline characterization data to develop vehicle handling models, which could be used in motion planning, and estimate the values of the model parameters for the different terrain types;
6. Analyze the driving perturbation maneuver data to estimate the model parameter values and to compare these to the values obtained in the baseline characterization;
7. Refine and formalize the driving perturbation maneuvers and analysis methods; and
8. Repeat the data collection and analysis on new terrain types to test the robustness and extensibility of the approach.

In the initial stage of the project we completed steps 1 through 4 and part of step 5 of the methodology.

3. DATA COLLECTION

3.1 Test vehicle and instrumentation

The test vehicle was an electric-powered, radio-controlled (R/C) $1/8^{th}$ scale truck, modified to operate under computer remote control (a PC issued steering and throttle radio-control commands) so that the driving commands could be precisely controlled and repeated. The R/C pulse-width modulation (PWM) format updates at 50 Hz (20 ms time blocks). Each 20 ms time block is divided into seven 3-millisecond blocks, which are decoded separately to control different devices and consist of a 1 ms "low" pulse, followed by a "high" pulse of variable duration from 1 to 2 ms (i.e., the analog servo motor command format). The test vehicle used only 2 channels: one for steering (going directly to a servo motor) and one for throttle (going to a speed controller).

The test vehicle, with instrumentation and the on-board data logger, is shown in Figure 1. The gross vehicle weight is 9 Kg and it has a 31-cm longitudinal wheelbase and a 29-cm lateral wheelbase, with 14.5-cm diameter tires. It has 4-wheel drive with front wheel Ackermann steering and 4-wheel independent suspension.

It operates on 14-Volt battery power and produces 65 N. of drawbar pull at stall with a 12-Volt throttle command. On flat asphalt, its sustained speed with a 12-Volt throttle command is 5.5 m/s. The drive train incorporated a slip clutch to limit shocks propagating through the drive train.

The vehicle was outfitted with two "outrigger" fifth wheels with digital rotary encoders. The fifth wheel contact centers were 58 cm apart. Each fifth wheel was connected to the vehicle with an undamped hinged joint allowing independent vertical motion. The fifth wheel data were used to estimate vehicle speed and turning radius. The vehicle was instrumented to record the voltage drop across the drive motor and the current through the drive motor. The latter was computed from the voltage drop across a 1% tolerance 1-ohm resistor in series with the motor. In steady state conditions, current through a DC motor is approximately proportional to torque and voltage drop is approximately proportional to angular speed. The vehicle was also equipped with two 3-axis linear accelerometers (+/- 6 g dynamic range) positioned on the centerline at the front and back of the vehicle equally spaced from the center of gravity. The accelerometers were 33.5 cm apart and were configured to provide estimates of pitch and yaw acceleration, in addition to 3-axis linear acceleration.

Data was recorded at 100 Hz with an on-board 8-channel data logger. Since there were 10 sensor channels, all of the data could not be captured on each run. The data was collected in two configurations. One configuration recorded the two rotary encoders, voltage drop across the motor, XYZ acceleration from the front 3-axis accelerometer and YZ from the rear accelerometer. The other configuration recorded the two rotary encoders, voltage drop across the motor, current through the motor, XYZ acceleration from the front 3-axis accelerometer and Y acceleration from the rear accelerometer.

3.2 Baseline characterization maneuvers

Three maneuvers were defined to collect baseline characterization data: (a) circling at constant steering and throttle command, (b) step function in throttle followed by a step to coasting, and (c) a step function in throttle followed by a step function to the reverse throttle setting.

The circling motion profile consisted of 3 seconds of linear increase in throttle to the cruising level, 8 seconds cruising at constant throttle, and 3 seconds linear decrease in throttle to zero. Only data from the 8 seconds at constant throttle were used in the analysis. The test maneuvers were conducted at four throttle levels (6, 8, 10 and 12 Volts) and three steering angles (10, 15 and 20 degrees).

Figure 1: Test vehicle on gravel terrain.

The throttle step-coast motion profile consisted of a step from throttle 0 to throttle X, cruising at throttle X for 3 seconds, then step to throttle zero. The test maneuvers were conducted at five throttle levels (6, 8, 10, 12 and 13 Volts) with neutral steering.

3.3 Provisional driving perturbation maneuvers

The driving perturbations were intended to be small deviations added to an underlying maneuver to measure vehicle response to braking, acceleration and steering commands. There were two throttle perturbations: pulsed throttle release and pulsed throttle reverse. There were two steering perturbations: a sine wave at constant amplitude and frequency, and a swept-frequency sine wave at constant amplitude. Sine wave perturbations in throttle and in steering amplitude were considered, but discarded after pilot testing. All maneuvers were to be conducted at four throttle levels (6, 8, 10 and 12 Volts).

The pulsed throttle release motion profile consisted of a step from throttle 0 to throttle X, cruising at throttle X for 3 seconds, step to throttle zero for 0.5 seconds, step back to throttle X for 2 seconds, then step to throttle zero. The test maneuvers were conducted with neutral steering.

The pulsed throttle reverse motion profile consisted of a step from throttle 0 to throttle X, cruising at throttle X for 3 seconds, step to throttle minus-X for 0.25 seconds, step back to throttle X for 2 seconds, then step to throttle zero. The test maneuvers were conducted with neutral steering.

The steering sine wave motion profiles consisted of a linear ramp to throttle X over 3 seconds, cruising at throttle X for 6 seconds with a steering sine wave. There were four cases with two steering sine wave amplitudes (10 and 15 degrees) and two periods (1.0 and 0.5 seconds).

The steering swept sine wave motion profiles consisted of a linear ramp to throttle X over 3 seconds, cruising at throttle X for 6 seconds with a steering swept sine wave with the period logarithmically increasing from 0.25 seconds to 4 second period. There were two cases with steering sine wave amplitudes of 10 and 15 degrees.

3.4 Field data collection

Data was collected on three types of terrain: an asphalt parking lot, a dirt/gravel road circular turn-around, and a rough field in an equestrian training area. Figure 1 shows the test vehicle on the dirt/gravel road terrain.

The asphalt parking lot was crowned to direct water run-off and was cracked in places. The dirt/gravel road was also crowned for water run-off. The gravel was not uniformly distributed, and the surface material in some parts was looser than in others. The rough field consisted of grass and weeds, unevenly mowed to a height of six to ten inches. The underlying ground was packed down by horses and was bumpy. At the scale of two meters or more, the field was relatively flat. However at the scale below one meter it had noticeable bumps and undulations. Data was collected in the autumn of 2003 under dry conditions.

Visual observation of the test runs and preliminary review of the data suggest several modifications to the throttle step response testing and to the steering swept sine wave frequency response testing. For on-the-fly testing, the perturbation has to produce detectable, but not disruptive, motion effects. In the steering swept sine wave testing, the perturbation appeared disruptive when the period exceeded one second. For on-the-fly testing, we can reduce the steering amplitude in proportion to the increase in period to avoid disruptive effects. The step response runs were conducted with neutral steering for a straight line trajectory. The runs had to be kept short to prevent the vehicle from exiting the test area. Consequently, we only capture one step – one data point – per run. Conducting the throttle step response testing in a fixed steering angle circling maneuver could allow us to collect multiple data points per run.

3.4 Data reduction

The raw accelerometer, current and voltage data were processed with a Hamming filter to smooth the data and reduce noise. The wheel encoder data contained large recurring unphysical steps, with one of the encoders much more prone to this error than the other. The data was corrected to eliminate these artifacts by taking first differences and removing large spikes. Wheel speed was determined by fitting a quadratic function at each point and computing the derivative.

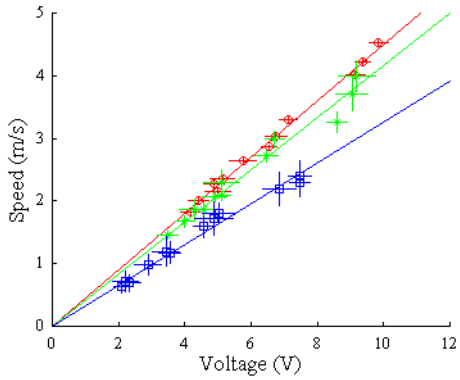

Figure 2: Speed versus voltage on asphalt (red circle), gravel (green star), and grass field (blue square).

4. MODELING AND ANALYSIS RESULTS

The results in this paper are limited to the circling maneuver and step-function data. Only data in the period of constant throttle was used in the circling analysis, while only the powered part of the step function data was analyzed. Using the circling data, we developed models of (1) speed, resistance and power consumption, (2) roll compliance, sideslip and turning radius, and (3) pitch and yaw disturbance. The step function data yielded results for ground resistance and maximum acceleration.

4.1 Steady state speed, resistance and power consumption

Under steady-state conditions, electric motor angular speed is approximately proportional to voltage. As expected, vehicle speed, v, was found to be approximately proportional to the voltage drop across the motor, V:

$$v = \alpha V, \qquad (1)$$

where α is a terrain-dependent constant. Model differences may be due to slip compounded by local spatial variations in the friction, resistance, and elevation of the terrain. Using the circling data, the model in (1) explains 99% of the variance in the data (Karlsen et al., 2004). Figure 2 shows a plot of the speed versus voltage data, with the weighted least squares fit to each data set. The steady state portion of the step function data yields similar results, with slightly larger constants, indicating that one achieves higher speeds at a given voltage when driving straight, rather than turning.

Under steady-state conditions, electric motor torque is approximately proportional to current. At constant speed, tractive force is equal to resistance, and tractive force is equal to torque divided by tire radius. Wong (Wong, 1993) suggests that resistance is proportional to speed squared, not proportional to speed, as is commonly

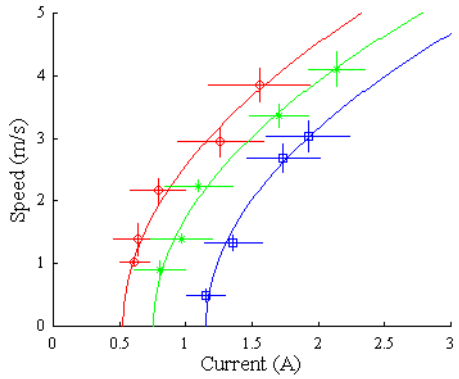

Figure 3: Speed versus current on asphalt (red circle), gravel (green star), and grass field (blue square).

assumed. Our data support the viscous resistance model in which current is a linear function of speed squared:

$$I = \beta v^2 + \gamma, \qquad (2)$$

where β and γ are terrain-dependent constants. The non-zero constant term in Equation (2) may be due to a combination of plastic deformation of the terrain, non-stationary surface properties, and internal resistance. Figure 3 shows plots of speed as a function of current for the three terrain types and five throttle settings (only 4 throttle settings for the rough field), along with the weighted least squares fit for each terrain type. The current data for the circling maneuver was collected only at 20 degrees steering angle. Over all 14 runs, the model explains 98% of the variance in the data with six free parameters.

The equilibrium data from the step function runs was consistent with the structure of Eq. (2), but yielded different constants. While the intercepts (γ) were similar between the two types of runs, the slopes (β) for the step function were a factor of two smaller, indicating that it takes significantly less current to reach the same speed traveling straight rather than turning.

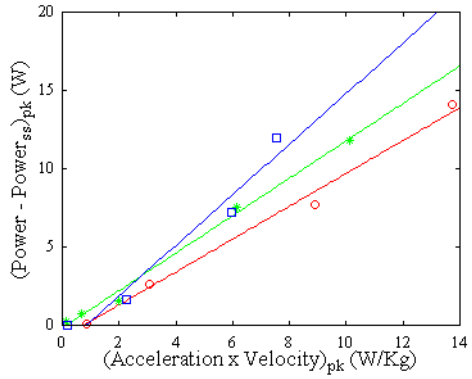

Figure 5: Acceleration power versus acceleration times velocity on asphalt (red circle), gravel (green star), and grass field (blue square).

Power equals current times voltage. Combining Equations (1) and (2) results in the following structure for power consumption as a function of velocity for steady state conditions:

$$P = v (\delta v^2 + \kappa), \qquad (3)$$

where δ and κ are terrain-dependent constants. The model explains 99% of the variance in the 14 data points from the circling data with six free parameters. Figure 4 shows the data, along with the weighted least squares fit for each terrain type. The step response data is again consistent with Eq. (3) but with different constants, indicating again that it requires more power to reach a given speed while turning than when traveling straight.

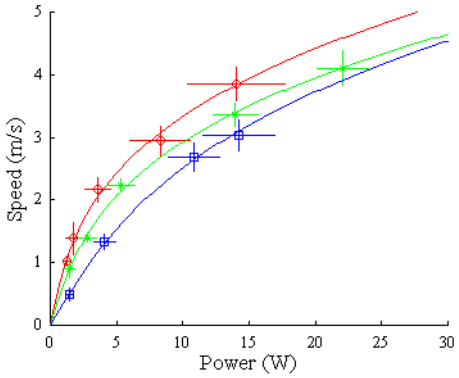

Figure 4: Speed versus power on asphalt (red circle), gravel (green star), and grass field (blue square).

4.2 Non-steady state power consumption

As stated above, the relationship between the steady state power and speed follows Eq. (3), both for the circling data and for the equilibrium portion of the step response data. Since the vehicle is presumed to be traveling on flat terrain, this represents the power required to overcome ground resistance and internal friction. For non-zero acceleration, the equation of motion becomes:

$$P = P_{ss} + m_{eff}\, a\, v, \qquad (4)$$

where P_{ss} is the steady state power from Eq. (3), m_{eff} is effective mass, and a is acceleration. The effective mass contains effects due to slip when accelerating and could also be termed acceleration effectiveness.

Figure 5 shows a plot of $P - P_{ss}$ versus a v, where P, P_{ss}, a, and v are taken at the point of maximum

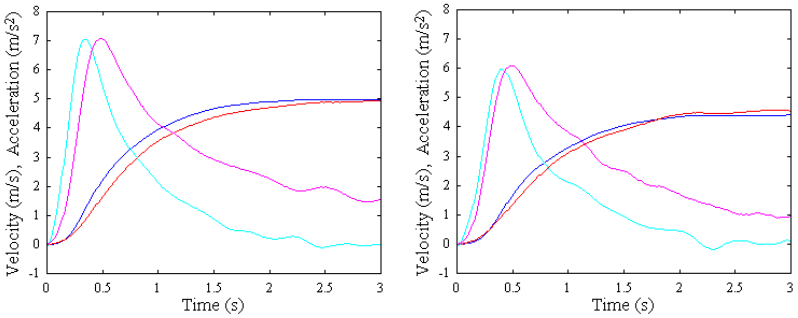

Figure 6: Solutions for velocity (blue) and acceleration (cyan) versus experimental velocity (red) and acceleration (magenta), for asphalt (left) and gravel (right). Experimental values for power.

acceleration. We subtract out the term P_{ss} because this deals with the effects of ground resistance, slip and internal resistance at a constant speed, while we are trying to isolate the effects of slip while accelerating. The slope of this plot gives a measure of the effective mass, which (in units of Kg) equals 1.05, 1.20 and 1.61 for the asphalt, gravel, and field terrain types.

Solving the differential equation in Eq. (4) provides velocity and acceleration as a function of time. Inputs are the constants δ and κ from Eq. (3) and m_{eff} from Eq. (4). We also employed two different solutions for the power P. In the first case, we used the measured values of P, as a function of time. Substituting these values into the differential equation and solving numerically results in the solution for v(t) shown in Figure 6. Differentiating v(t) yields the solution for a(t). Comparisons are made to the experimental values for v(t), found from the wheel encoders, and a(t), as measured by the accelerometers. We note that the experimental measurements for a(t) in Figure 6 have been scaled by a factor of 0.8. This correction factor is determined by plotting the peak acceleration versus the steady state acceleration (which should be zero). The vehicle tilts back while moving due to the vehicle's suspension compliance and therefore, the measured forward acceleration has a constant component due to gravity that is proportional to the force required to overcome terrain resistance.

A second solution for v(t) is found by using a simple model for the power,

$$P = P_{inf}\,(1 + \tanh(10t - 4.5))/2, \qquad (5)$$

where P_{inf} is the steady state power and is obtained from the data for each speed and terrain type. The numerical constants in the model are chosen such that the time to reach half power and the slope at half power are similar to data. The maximum acceleration time of t=0.45 s is relatively constant for all speeds and terrain types. Figure 7 shows the results of solving the resulting differential equation for the velocity, which is compared to the experimental speed found from the wheel encoders. Differentiating the velocity results in the modeled acceleration, which is compared to the output of the accelerometers. These results look reasonably promising and capture the overall structure of the speed profile.

4.3 Roll compliance, sideslip and turning radius

Theoretically, lateral acceleration is equal to speed squared, divided by the turning radius. Acceleration in the body Y direction, A_Y, as measured by the accelerometers was approximately equal to a gain times this theoretical lateral acceleration. Roll compliance accounts for the difference:

$$A_Y = (\,v^2 / R\,)\cos(\,\chi\,) + g\sin(\,\chi\,), \qquad (6)$$

where v is the speed, R is the turning radius, g is the acceleration due to gravity, and χ is the roll angle. The roll angle is a function of the lateral acceleration, v^2 / R, and the roll compliance, η, of the vehicle (Gillespie, 1992):

$$\sin(\,\chi\,) = \eta\, v^2 / R\,. \qquad (7)$$

Figure 8 shows a plot of the mean lateral accelerometer measurement versus mean v^2 / R estimate. The model explains 98% of the variance in the 36 data points. Vehicle speed was estimated by averaging the inner and outer fifth wheel velocities. The turning radius was estimated from the relative speeds of the inner and outer fifth wheels.

During cornering, the vehicle experiences sideslip, which causes the effective turning radius to increase.

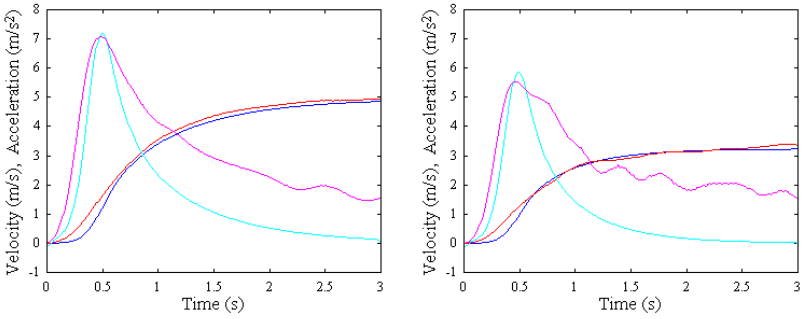

Figure 7: Solutions for velocity (blue) and acceleration (cyan) versus experimental velocity (red) and acceleration (magenta), for asphalt (left) and grass field (right). Model values for power.

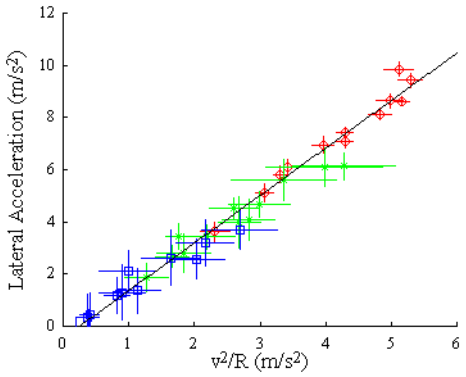

Figure 8: Lateral accelerometer output versus v^2/R asphalt (red circle), gravel (green star), and grass field (blue square).

Sideslip occurs when the lateral acceleration is greater than the opposing friction. The frictional force at an instant in time and space is commonly modeled as a coefficient of friction between the two materials times the normal load (or normal force between them).

The asphalt surface was relatively smooth, even and uniform. Consequently, we expect that the normal load on the four tires, the coefficient of friction, and the resulting frictional force opposing sideslip, would all be relatively constant. Therefore, we expect no sideslip until the lateral force exceeds the opposing friction, whereupon the turning radius will increase to the point where the lateral force just equals the opposing friction. This coulomb friction model leads to the following equation for the turning radius:

$$R = \max\{ K / \tan(\theta),\ v^2 / \mu g \}, \qquad (8)$$

where K is a vehicle constant, θ is the steering angle, v is speed, μ is the coefficient of sliding friction and g is the acceleration due to gravity. Until sideslip occurs, the turning radius is independent of velocity, depending only on the steering angle. Thereafter, the turning radius increases as the square of the velocity, independent of the steering angle.

The dirt/gravel road and the rough field were uneven surfaces with varying surface conditions. Due to uneven terrain and vehicle dynamics, the vehicle would experience pitch and heave, producing varying normal loads on the tires. The coefficient of friction also varies depending on how large and loose the road surface particles are, and the length, density and type of the mowed grass and weeds. Variations in normal load and variations in the coefficient of friction produce variations in the magnitude and frequency of sideslip. In these cases, the effective parameters in Equation (8) are expected to capture the average properties of the vehicle-terrain interaction.

Figures 9 show the measured turning radius as a function of the average vehicle speed squared for the asphalt surface. As expected, the coulomb friction model gives a very good estimate of turning radius (Karlsen et al., 2004), explaining 98% of the variance between the model and data. The model for the gravel terrain captured less of the data variations, while the rough grass field model provided the worse fit. Ideally, the parameter K should be independent of terrain and depend only on geometric aspects of the vehicle, but this was not the case due to over-steer and/or under-steer conditions. The value derived from the asphalt is expected to be more reliable since the other terrain surfaces caused substantial disturbance in the vehicle's circular path.

4.4 Pitch and yaw disturbance magnitude

Pitch and yaw disturbance was estimated from the difference in the outputs of the front and rear Z and Y accelerometers respectively, divided by the distance between them. We used the same functional form to model the standard deviation of the pitch and yaw disturbance as a function of speed and steering angle:

$$D = v\,(\rho + \sigma \sin(\theta)), \qquad (9)$$

where D is the disturbance, v is speed, θ is the steering angle, and σ and ρ are terrain-dependent constants. The values of σ and ρ are assumed to be different for pitch and for yaw. The pitch model and data for the gravel terrain is shown in Figure 10. The pitch model was able to explain 96% of the variance in the 36 data points with six free parameters.

The yaw model was able to explain 93% of the variance in the 36 data points with six free parameters. Note that the pitch disturbance for the field terrain is largely steering angle independent and the yaw

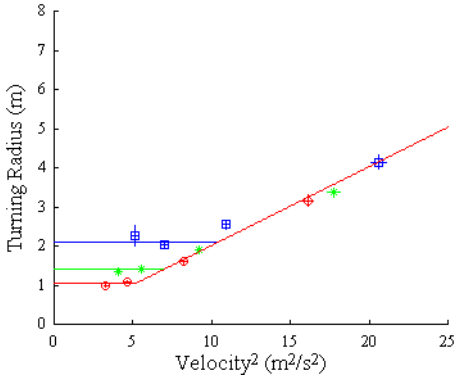

Figure 9: Turning radius versus velocity squared as a function of steering angles of 20º (red circle), 15º (green star), and 10º (blue square) on asphalt.

disturbance for the asphalt is primarily steering angle dependent. Adding a velocity squared term would potentially increase the correlation, although at the expense of an additional free parameter, but is likely to remain a second order effect.

5. OBSERVATIONS AND CONCLUSIONS

The described approach employs the UGV as a test instrument to collect data on its own handling characteristics. Consequently, the values of the model parameters will be specific to that vehicle. It is possible that that the model equations themselves have limited applicability to other UGV configurations and running gear. For example, the equations might well apply to other Ackermann-steer wheeled vehicles, and might even apply to skid-steer tracked vehicles (with some modification for the different driving control parameters), but are unlikely to apply to legged walking systems.

We propose to measure response to steering, braking and throttle commands by introducing small perturbations to analyze frequency response and step response. The perturbations must be large enough to produce measurable response, but not so large as to introduce deviations that interfere with the ongoing maneuver. Our observations on different terrain suggest that perturbations that produce just measurable effects on one terrain (e.g., rough field) may be disruptive on another terrain (e.g., asphalt), and perturbations that produce near-disruptive effects on one terrain (e.g., asphalt) may not produce detectable effects on another (e.g., rough field). This suggests an adaptive approach in which the magnitude of the perturbation is increased until the magnitude of the effects reaches some threshold.

Vehicle speed is a key factor in the models of power consumption, sideslip and disturbance. The UGV needs to be able to reliably measure its ground speed. We employed wheel encoders on non-drive wheels. If this option is not available, some other means to estimate ground speed is needed.

Our preliminary results suggest that simple models of power consumption and disturbance as a function of speed are adequate and can easily be specified from vehicle motion data. Sideslip, turning radius, and acceleration depend on the effective friction, which poses problems. The differential equation for velocity as a function of time, along with the power model, appears to have captured the gross structure of the velocity profile of the vehicle. We have not yet analyzed the braking runs and these results may shed more light on the appropriate model for friction and slip.

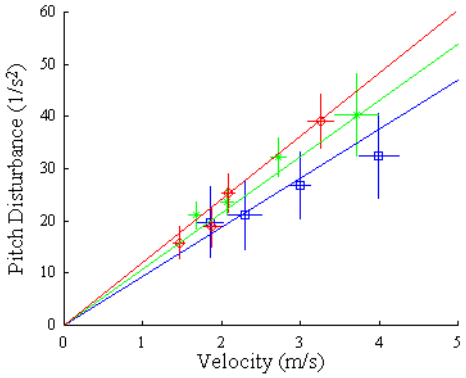

Figure 10: Pitch disturbance versus velocity as a function of steering angles of 20º (red circle), 15º (green star), and 10º (blue square) on gravel.

Our approach to date has been to measure handling response, just as a human driver assesses response to driving commands. Human drivers also judge handling limits based on the feel of the road, i.e., the ground disturbance. Ground disturbance is easy to measure and is both a contributing cause and collateral consequence of other aspects of vehicle terrain interaction. The three terrain types were clearly distinguished by the disturbance magnitude. It is possible that many vehicle handling characteristics could be predicted simply from disturbance measurements. This would require assembling a database of disturbance and vehicle handling data for a variety of terrain types, and building an associative relationship between the two. The benefit of this complementary approach is that it would produce initial handling estimates even when there is no time for the driving perturbation exercises.

REFERENCES

Birkel, P.A., "Terrain trafficability in modeling and simulation," SEDRIS Technical Paper 1 (2003).

Brooks, R.A., "How to build complete creatures rather than isolated cognitive simulators," in K. VanLehn (ed.), *Architectures for Intelligence*, Lawrence Erlbaum Assosiates, Hillsdale, NJ, 225-239 (1991).

Gillespie, T.E., *Fundamentals of Vehicle Dynamics*, Society of Automotive Engineers, Warrendale, PA (1992).

Karlsen, R.E., G. Witus, and J.L. Overholt, "On-the-fly assessment of terrain effects on UGV handling," *Unmanned Ground Vehicle Technology VI*, eds. G.R. Gerhart, C.M. Shoemaker, and D.W. Gage, SPIE Proc. 5422, 484-92 (2004).

Wong, J.Y., *Theory of Ground Vehicles, 2nd Edition*, John Wiley and Sons, New York, NY (1993).